Simulation of Near Field RCS to Reproduce Measurement Condition

Jose M. Tamayo-Palau [#1], Pascal de-Resseguier[#2]

[#]NEXIO, Toulouse, France

{[1]jose-maria.tamayo-palau, [2]pascal.de-resseguier}@nexiogroup.com

***Abstract* — Different approaches are presented to simulate the near field Radar Cross Section (RCS) of a perfectly conducting electrically large object. This type of environment is usually found in measurements at large anechoic chambers where the far field condition cannot be achieved, making it impossible to approximate the incident field by a planewave. Each approach will be implemented with Physical Optics (PO) for extremely large targets and an accelerated version of the Method of Moments for moderately large objects. The fast MoM method are either the Multilevel Adaptive Cross Approximation (MLACA) for an iterative solution or the Multiscale Compressed Block Decomposition (MSCBD) for a direct solution. This development and the performed simulations have been done with CAPITOLE-RCS commercial software developed by NEXIO.**

***Keywords* — Numerical simulation, radar cross-sections, method of moments, physical optics, anechoic chambers, inverse synthetic aperture radar.**

I. Introduction

Several applications include the RCS characterization of electrically large objects which are placed at a finite distance from the transmitting and receiving antennas, smaller than the far field condition. These include the measurement of an airplane in a large anechoic chamber, where the object under analysis can cover almost all the chamber [5]-[9]. This is why a RCS definition in the near range has been introduced, from here on called near field RCS. Several authors have published some papers in order to infer this value from a simulation, by the use of a spherical incident wave and PO [1]-[4]. This approach is extremely efficient but it has also some limitations in terms of precision depending on the complexity of the object.

To avoid these limitations, we have implemented the same approach but using a couple of fast methods based on the MoM instead of PO to get the surface induced currents on the object. In particular, we can choose either the MLACA [10] or the MSBCD [11]. In addition, we have developed another approach which represents better what is done in a measure environment and will allow us to validate both procedures from a numerical point of view. This technique uses sets of dipoles as transmitting and receiving antennas and calibrates afterwards with the values of a known object such as a sphere.

Section III presents some numerical results to test the approaches. In some cases, we have also performed a Near Field to Far Field (NF2FF) transformation [12] from the near results and compare it with the far field simulation or even an ISAR image in the last test case.

The novelty of this paper resides in the fact of using the rigorous MoM instead of a high frequency PO method as well as including a comparison of two quite different approaches to model a near field RCS measurement environment. Furthermore, the MoM solution is accelerated and compressed with the iterative MLACA fast method and the direct MSCBD method.

II. Near field RCS computation

Our aim is to simulate a measurement environment, such as an anechoic chamber under the consideration of being in the near field range of the receiving and transmitting antennas. Fig. 1 shows a schema of this scattering problem. Two approaches are proposed which will be compared in section III with some examples.

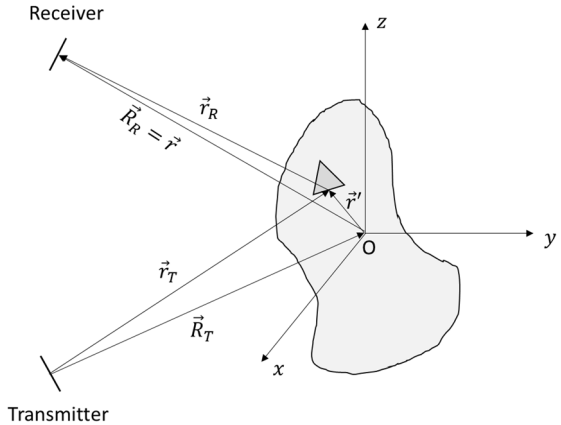

Fig. 1. Geometry of the scattering problem under study.

A. Approach 1: Spherical Wave Source and Near Field RCS

The first approach tries to generalize the far field RCS concept where a planewave incident field is considered to the near field case. According to [1] , the planewave incident field can be substituted by a spherical wave whose electric and magnetic fields can be expressed as:

$$\vec{E}^i(\vec{r}') = \frac{e^{-jkr_T}}{r_T}\hat{e}_i \quad (1)$$

$$\vec{H}^i(\vec{r}') = \frac{1}{\eta}\frac{e^{-jkr_T}}{r_T}\hat{h}_i, \quad (2)$$

where η is the free space wave impedance, and $\hat{e}_i$, $\hat{h}_i$ are the polarization vectors of the electric and magnetic incident fields,

respectively. Notwithstanding, a generalization of the RCS to the near field range is expressed in the following formula based on the electric and magnetic scattered fields $\vec{E}^s(\vec{r})$ and $\vec{H}^s(\vec{r})$:

$$\sigma_{NEAR} = 4\pi R_R^2 \frac{|\vec{E}^s(\vec{r})\times\vec{H}^s(\vec{r})^*|}{|\vec{E}^i(\vec{r})\times\vec{H}^i(\vec{r})^*|}. \quad (3)$$

The previous expression is hardly tractable, but can be simplified with the approximations commented in [1] by:

$$\sigma_{NEAR} \approx 4\pi R_T^2 R_R^2 \eta^2 \left|e^{jk(R_R+R_T)}\vec{H}^s(\vec{r})\right|^2 . \quad (4)$$

The magnetic scattered field is then computed with the well-known formula:

$$\vec{H}^s(\vec{r}) = \int_S \nabla G(\vec{r}_R) \times \vec{J}(\vec{r}')\, ds', \quad (5)$$

where G is the free space Green function

$$G(\vec{r},\vec{r}') = \frac{e^{-jkR}}{4\pi R} \quad (6)$$

whose gradient can be developed into:

$$\nabla G(\vec{r},\vec{r}') = (1+jkR)\frac{G}{R^2}. \quad (7)$$

We propose two ways for computing the surface current $\vec{J}(\vec{r}')$ on the object. The first option is to use a high frequency Physical Optics (PO) method as is done in most of the references. In this case, the expression of the currents is straightforward with the following

$$\vec{J}(\vec{r}') = \begin{cases} 2\hat{n}\times\vec{H}^i(\vec{r}') & ,lit\ region \\ 0 & ,shadow\ region \end{cases} \quad (8)$$

where $\hat{n}$ is the normal to the surface of the object at each point. Although the PO method is highly approximated, it is nevertheless the only choice for extremely large objects, where more rigorous methods would be very inefficient and would demand a vast range of resources.

The second proposed option is to use the Method of Moments, where the currents are discretised with the RWG basis functions defined over each pair edge-touching triangles:

$$\vec{J}(\vec{r}') = \sum_n J_n \vec{f}_n(\vec{r}'). \quad (9)$$

In order to get the coefficients for the currents we need to solve a linear dense system:

$$[Z_{mn}][J_n] = [\mathrm{E}_m] \quad (10)$$

whose matrix elements are the usual EFIE ones whereas the right-hand side should be updated with the new electric incident field (spherical wave)

$$E_m = \langle \vec{E}^i, \vec{f}_m \rangle = \int_S \vec{E}^i(\vec{r}')\cdot\vec{f}_m(\vec{r}')\, ds'. \quad (11)$$

As the storage and the solution of the MoM system grows rapidly with the electrical size of the problem, it is necessary to use a fast method such as MLFMM, MLACA which are iterative methods, or the MSCBD or H-matrix which are direct methods. In our case we have developed MLACA and MSCBD in order to compressed and accelerate the solution.

B. Approach 2: Dipole Source and Receiving Antenna with Normalization

In the second approach we consider as transmitting and receiving antenna an elementary dipole or a set of dipoles. According to [5] the radiated field of an antenna can be approximated by a set of well distributed infinitesimal dipoles making this choice a quite general approach.

The radiated field from the dipole, and therefore the incident field in the object, in spherical coordinates where the spherical coordinate system is placed and oriented at the emitting dipole can be expressed as:

$$H_\phi^i = j\frac{I\delta l}{4\pi}\left(\frac{k}{r}-\frac{j}{r^2}\right)e^{-jkr}\sin(\theta) \quad (12)$$

$$E_\theta^i = j\frac{\eta I\delta l}{4\pi}\left(\frac{k}{r}-\frac{j}{r^2}-\frac{1}{kr^3}\right)e^{-jkr}\sin(\theta) \quad (13)$$

$$E_r^i = \frac{\eta I\delta l}{2\pi}\left(\frac{1}{r^2}-\frac{j}{kr^3}\right)e^{-jkr}\cos(\theta). \quad (14)$$

Next, we compute the surface currents induced in the object J. Both PO or MoM (MLACA or MSCBD) based method could be used to compute the surface currents as in the first approach.

Afterwards we compute the electric field radiated or scattered from these surface currents at the position of the receiving antenna dipole. In particular, only the component of the field polarized with the dipole antenna is considered. The same electric near field calculation is performed with a calibration object whose RCS is known, in our case a sphere with size similar to the actual object under study. Then we compute the near field RCS as

$$\sigma_{NEAR} = \frac{|\vec{E}^s(\vec{r})|}{|\vec{E}^s_{SPHERE}(\vec{r})|}\sigma_{SPHERE} \quad (15)$$

where the scattered electric field is computed by using the Dyadic Green function

$$\bar{\bar{G}}(\vec{r},\vec{r}') = \left[\bar{\bar{I}} + \frac{\nabla\nabla}{k^2}\right]G(\vec{r},\vec{r}') \quad (16)$$

with the expression:

$$\vec{E}^s(\vec{r}) = -jk\eta\int_S \bar{\bar{G}}(\vec{r},\vec{r}')\cdot\vec{J}(\vec{r}')\, d\vec{r}' \quad (17)$$

$$\vec{E}^s(\vec{r}) = -jk\eta\int_S \left[\left(\frac{3}{k^2R^2}+\frac{3j}{kR}-1\right)\left(\hat{R}\cdot\vec{J}(\vec{r}')\right)\hat{R} + \left(1-\frac{1}{k^2R^2}-\frac{j}{kR}\right)\vec{J}(\vec{r}')\right]G(\vec{r},\vec{r}')\, ds'. \quad (18)$$

This expression can be further simplified in the case of the MoM with RWG basis functions.

III. Numerical results

C. PEC Cylinder with Shifted Antennas

The geometry for the first test case is shown in Fig. 2. It corresponds to a cylinder of length 2.6m and diameter 0.4m at 14GHz. The transmitting and receiving antennas have an elevation shift of 12° and -28° with respect to the XY plane. The transmitting antenna is placed at a distance 54.64m and the receiving one at 24.82m. The cylinder turns horizontally over the Z axis between -5° and 5°.

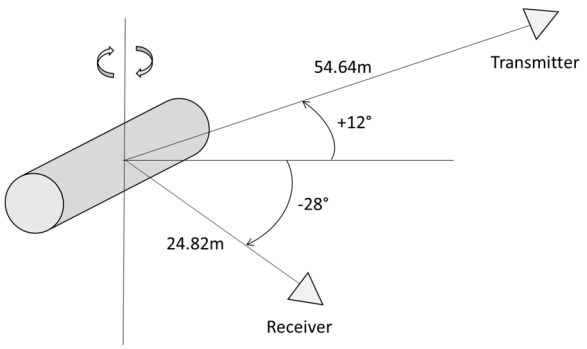

Fig. 2. Near Field bistatic RCS configuration of a perfectly conducting cylinder of length 2.6m and diameter 0.4m at 14GHz.

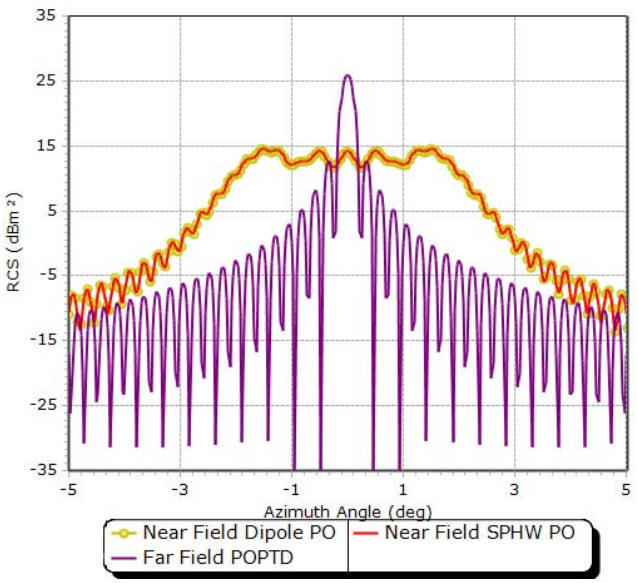

Fig. 3. Near Field and Far Field bistatic RCS results of a perfectly conducting cylinder of length 2.6m and diameter 0.4m at 14GHz.

Fig. 3 show the resulting RCS for this case. Three simulations have been performed: near field RCS using the second approach with PO to compute currents (Near Field Dipole PO in the figure), near field using the first approach with PO to compute currents (Near Field SPHW PO in the figure) and far field RCS using POPTD method considering the antennas have no elevation shift. The results perfectly agree with the ones obtained in [1]. The near field RCS obtained with the two approaches are equal as well.

D. PEC Circular Disc

In this second test case the antennas have no elevation shift and are both placed at a distance 18m. The rotating object corresponds to a circular disc with diameter 1.128m at 17GHz. It has been discretized into 789285 unknowns. The disc is placed so that the central point corresponds to the normal angle of incidence.

Fig. 4 shows the resulting RCS. Four simulations are performed: near field RCS using the first approach and MoM-MLACA to compute the currents (Near Field MLACA in the figure), near field using the first approach and PO to compute the currents (Near Field SPHW PO in the figure), and far field using either the MLACA method or the POPTD method (Far Field MLACA and Far Field POPTD, respectively). The results match with the ones in [3]. A good agreement is also obtained, both in the far and near field RCS, between using MoM-MLACA method or PO method. This is because the disc is well suited for planar objects.

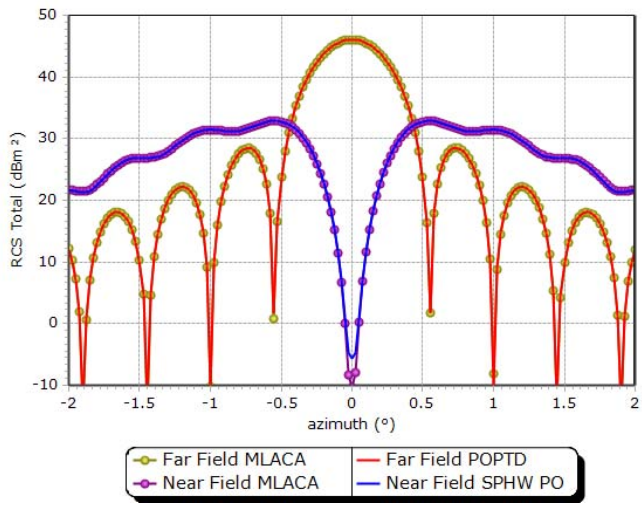

Fig. 4. Near Field and Far Field monostatic RCS results of a perfectly conducting circular disc of diameter 1.128m at 17GHz.

E. PEC Rectangular Plate

With the same configuration as the previous case we have simulated a rectangular plate with dimensions 1mx0.2m at 8GHz.

Fig. 5 shows the resulting RCS for this case. Three curves are shown. One for the near field RCS using the first approach with MoM-MSCBD method to compute the currents, far field RCS using MoM-MSCBD method and the far field RCS obtained with a NF2FF transformation technique [12] from the near field RCS result. Both far field values perfectly agree except on the extreme angles. This is due to a limitation of the used NF2FF algorithm and could be avoided by incrementing the azimuth range of the near field RCS result.

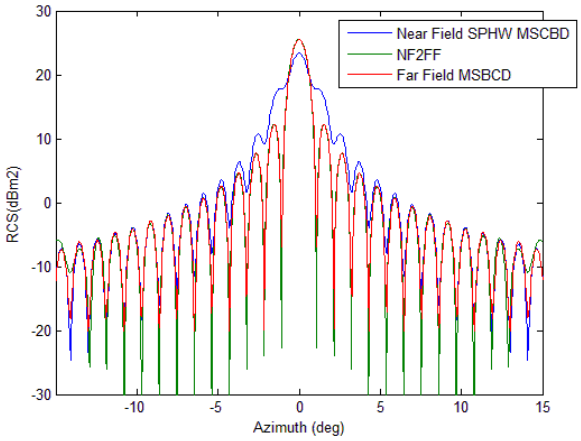

Fig. 5. Near Field, Far Field and recovered Far Field from Near Field monostatic RCS results of a perfectly conducting rectangular plate of length sides 1m x 0.2m at 8GHz.

F. PEC Cylinder Monostatic

The last test case uses the same configuration as the previous case but with the antennas placed at a distance 18.6m. Instead of a rectangular plate we analyze a cylinder with length 2.605m and diameter 0.45m.

Fig. 6 shows the resulting RCS at 8GHz and 12GHz. In this case PO is used in both near and far field RCS computations. We have also included the far field by the use of a NF2FF algorithm from the near field RCS result. The same conclusions as in the previous case apply.

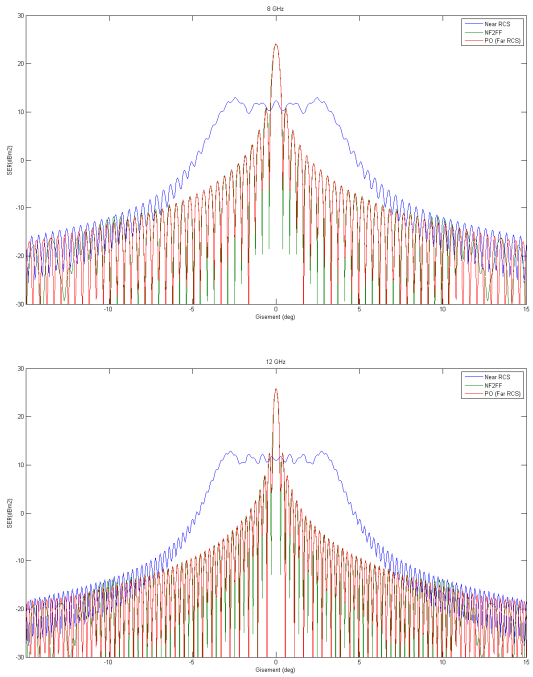

Fig. 6. Near Field, Far Field and recovered Far Field from Near Field monostatic RCS results of a perfectly conducting cylinder of length 2.605m and diameter 0.45m at 8GHz and 12GHz (from top to bottom).

Furthermore, we have got an ISAR image in the three cases (frequency sweep between 8GHz and 12.4GHz) shown in Fig. 7. We can observe the usual bending in the near field measure (in the center of the figure), which is properly removed when using the NF2FF algorithm.

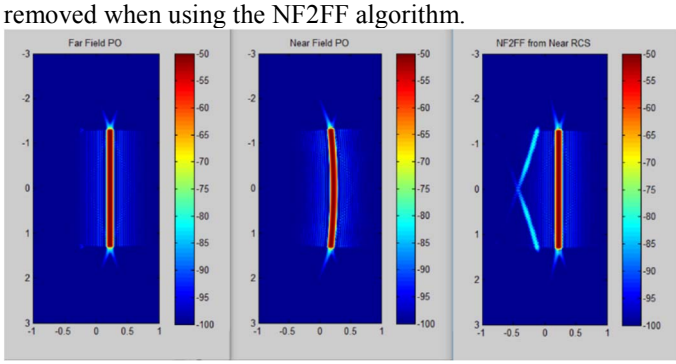

Fig. 7. ISAR image obtained from the Far Field (left), from the Near Field (center) and from the recovered Far Field from Near Field (right) monostatic RCS results of a perfectly conducting cylinder of length 2.605m and diameter 0.45m.

IV. Conclusion

Two distinct methods have been developed to approximate the near field RCS of targets using in each one either the MoM (rigorous) or the PO (high frequency) methods. When the complexity of the object increases, the PO method becomes inaccurate making the MoM procedure a good choice. Thanks to some numerical experiments we have tested each one of the approaches.

References

[1] P. Pouliguen, J.F. Damiens, R. Hemon and J. Saillard, “RCS computation in near field,” *DAYS on DIFFRACTION 2006*, St. Petersburg, 2006, pp. 252-265.

[2] P. Pouliguen, R. Hemon, C. Bourlier, J.F. Damiens and J. Saillard, “Analytical Formulae for Radar Cross Section of flat plates in Near Field and Normal Incidence,” *Progress In Electromagnetics Research B,* vol. 9, pp. 263-279, 2008.

[3] P. Pouliguen, and L. Desclos, “A physical optics approach to near field RCS computations,” Ann. Télécommun. (1996) 51: 219.

[4] S. R. Legault, “On Near-Field Computations Using Physical Optics,” *URSI EMTS* 2004, pp. 33-35.

[5] B. Dulucq, S. Morvan, P. Massaloux and G. Mazé-Merceur, "Near-field 3D-RCS measurement simulation: Antenna pattern issues," *The 8th European Conference on Antennas and Propagation (EuCAP 2014)*, The Hague, 2014, pp. 3225-3227.

[6] Y. Chevalier, G. Maze-Merceur, S. Morvan, P. Bonnemason and A. Menard, “RCS measurement of large scale target in the V/UHF range: Analysis of the performances of SOLANGE facility,” AMTA 2003.

[7] G. Maze-Merceur, S. Morvan and P. Bonnemason, “RCS measurement in an anechoic chanmber in the U/VHF band: Comparison with experimental 1:10 scale simulation,” AMTA 2000.

[8] G. Maze-Merceur and P. Bonnemason, “RCS measurement in an anechoic chamber in the V/UHF band: ray tracing model and exact simulation,” AMTA 2001.

[9] L. Le-Dem, “SOLANGE an enhanced RCS measurement facility of full size aircraft,” AMTA 2003.

[10] J. M. Tamayo, A. Heldring and J. M. Rius, "Multilevel Adaptive Cross Approximation (MLACA)," in *IEEE Transactions on Antennas and Propagation*, vol. 59, no. 12, pp. 4600-4608, Dec. 2011.

[11] A. Heldring, J. M. Rius, J. M. Tamayo, J. Parrón and E. Ubeda, "Multiscale Compressed Block Decomposition for Fast Direct Solution of Method of Moments Linear System," in *IEEE Transactions on Antennas and Propagation*, vol. 59, no. 2, pp. 526-536, Feb. 2011.

[12] T. Guillemot, “Correction des effets de champ proche appliquee a des mesures de SER,” PhD Thesis, Ecole Doctorale Sciences pour l'Ingenieur de Nantes, September 1995.